

## Ionization Processes and Charge-State Distribution in a Highly Ionized High- $Z$ Laser-Produced Plasma

M. E. Foord, S. H. Glenzer, R. S. Thoe, K. L. Wong, K. B. Fournier, B. G. Wilson, and P. T. Springer

*University of California, Lawrence Livermore National Laboratory, Livermore, California 94551*

(Received 3 February 2000)

The charge-state distribution in a well-characterized highly ionized Au plasma was accurately determined using time-resolved x-ray spectroscopy. Simultaneous measurements of the electron temperature and density allow the first direct comparisons with nonlocal thermodynamic equilibrium model predictions for the charge-state distribution of a highly ionized high- $Z$  plasma in a nonradiative environment. The importance of two-electron atomic processes is clearly demonstrated.

PACS numbers: 52.25.Jm, 52.25.Nr, 52.50.Jm, 52.70.La

Nonlocal thermodynamic equilibrium (non-LTE) processes control the behavior and macroscopic conditions of high temperature plasmas generated in many present day experiments such as in hohlraums [1], tokamaks [2], and  $Z$  pinches [3], as well as astrophysical sources [4]. In such plasmas, emission spectra are often used as a means for diagnosing plasma conditions and for studying a wide variety of plasma phenomena. Although much progress has been made in the study of  $K$ -shell and  $L$ -shell spectra [5,6], little work has focused on understanding non-LTE processes in the more complex  $M$ - and  $N$ -shell atomic systems [7,8]. This is of particular importance for high power devices such as hohlraums and  $Z$  pinches, where high- $Z$  ( $Z > 50$ ) materials are typically used and where the electron temperature is often sufficient to reach highly ionized states. In this Letter, we present results in which the density, temperature, and charge-state distribution in a hot Au plasma are determined independently, allowing the first direct comparisons to predictions from non-LTE models in this highly ionized high- $Z$  regime.

In general, a balance between collisional and radiative processes such as ionization, recombination, excitation, and radiative decay governs the degree of ionization in a non-LTE plasma. In high- $Z$  materials ionized into open  $M$ - or  $N$ -shell configurations, two electron processes play an important role by adding significant channels for ionization and recombination through multiply excited states. Such two-electron processes consist of resonant capture into a doubly excited state and its inverse, autoionization. Resonant capture can also be stabilized by radiative decay of one of the excited electrons leading to dielectronic recombination. In most cases, these complex systems of levels and transitions are too numerous to treat in full detail. This has led to a number of approximate theoretical approaches such as average atom models, e.g., XSN [9], hydrogenic detailed configuration accounting models, and more detailed models such as SCROLL [10], MCUTA [11], and FINE [12]. In fact, predictions for the average charge from various non-LTE models for  $M$ -shell Au have recently been shown to disagree by more than ten ionization stages [13], emphasizing the need for well-characterized

experimental data. Accurate data may also test current theories, which rely on LTE distributions [14].

Recent experiments on a laser-heated Au disk have indicated the importance of including dielectronic recombination in modeling the conditions of the blow-off plasma [8]. A more direct approach for testing atomic models is to produce a plasma with uniform, slowly varying conditions, and independently measure the density, temperature, and charge-state distribution. In this Letter, we describe experiments where Au microdot samples, buried in a thin Be foil, are laser heated to 2 keV ( $2.3 \times 10^7$  K) and ionized into the  $M$  shell. Samples are well tamped to provide the high densities required for steady-state ionization equilibrium and to maintain uniform conditions during expansion. The electron density is determined by x-ray imaging the Au sample, and the electron temperature is measured with Thomson scattering. The charge-state distribution is obtained from analysis of temporally resolved measurements of  $5f$ - $3d$  x-ray emission spectra, allowing the average charge  $Z^*$  to be determined to within  $\sim 1\%$  accuracy. To our knowledge, these results provide the first accurate determination of the charge-state distribution in a highly ionized high- $Z$  plasma. As presented below, model predictions that include two-electron processes are consistent with the data, and the effect of including these processes on the charge-state distribution are significant.

These experiments were conducted on the NOVA laser facility at Lawrence Livermore National Laboratory [15]. The targets consisted of 1-mm-square, 12- $\mu$ m-thick Be foils with 200- $\mu$ m-diameter 1000- $\text{\AA}$ -thick layers of Au centrally buried in the foil. The foils are heated with 8 ns, flat-top (100 ps rise time),  $\approx 2$  kJ, 350 nm beams from each side. The beams are spatially smoothed, resulting in uniform illumination over a 350- $\mu$ m-diameter circular focal spot. Two beams are centrally focused on each side, overfilling the buried Au region, while seven beams are distributed to fully ionize the surrounding Be foil.

The electron temperature was measured with a Thomson scattering diagnostic [16]. The 263-nm, 50-J, 4-ns-long probe laser was directed normal to the target and focused to a 100- $\mu$ m-diameter spot at target center. The critical

electron density of the probe is  $n_e = 1.7 \times 10^{22} \text{ cm}^{-3}$ , allowing the plasma to be probed early during its expansion, when its density is high and when the plasma is near steady-state ionization equilibrium. Light is collected at  $90^\circ$  from  $\sim(100 \mu\text{m})^3$  scattering volume and relayed to a spectrometer coupled to a streak camera detector system that records the time-dependent spectrum of scattered light with 30 ps resolution. X-ray imaging data indicates that, within a few nanoseconds, the sample has expanded sufficiently such that the scattering volume should be well within the Au sample and not affected much by the surrounding Be tamper material. The spectrum consists of two clearly defined ion-acoustic features that are separated by twice the ion sound speed, proportional to  $(Z^*T_e)^{1/2}$  (see Fig. 1). The spectrum is fitted using theoretical predictions of Thomson scattering [16] that include beam broadening of the ion acoustic peaks due to the transverse velocity gradient predicted from LASNEX [17] simulations. The asymmetric profile suggests a shift in the electron distribution function, possibly due to heat flow. As described below,  $Z^*$  is determined directly from the emission spectrum and this determination is only weakly dependent on  $T_e$ . This yields an electron temperature  $T_e \cong 2.2 \text{ keV} \pm 10\%$ , using  $Z^* = 49$  as derived below from the Au emission spectrum. The uncertainty in  $T_e$  arises mainly from the accuracy in determining the separation of the ion-acoustic features due to noise in the data. In one experiment where the probe beam energy was much lower (25 J), the plasma reached similar conditions, suggesting that the probe contributes little to the sample heating.

The density was obtained from spatial imaging the x-ray emission to determine the extent of the sample expansion. The x-ray spectrometer (described below) views the sample side-on and spatially images parallel to the foil surface. Side-on and face-on x-ray pinhole images of the Au emission are also recorded with time-gated channel plate detectors on film. The Au sample expands mainly

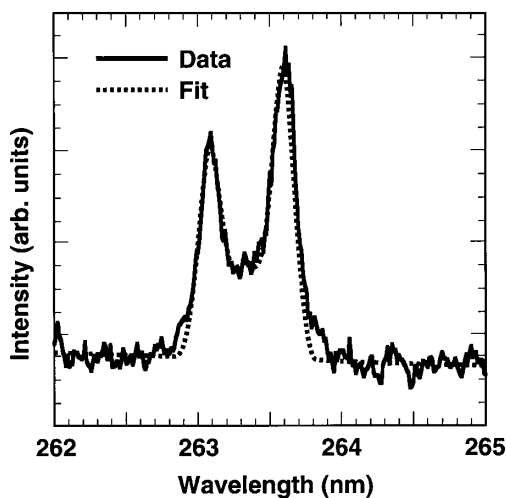


FIG. 1. Thomson scattering data at  $\approx 3$  ns following the laser initiation shows well-resolved ion-acoustic features. The dotted line is a theoretical fit corresponding to  $T_e = 2.2 \text{ keV}$ .

in the axial direction normal to the surface, and reaches  $n_e = 6 \times 10^{20} \text{ cm}^{-3} \pm 20\%$  ( $400 \mu\text{m}$  axial expansion) at 2.8 ns after the laser initiation, coincident to the Au spectrum presented below.

The laser heating and hydrodynamic expansion were simulated with the 2D hydrodynamic code LASNEX [17]. The density in the thin Au layer remains uniform during expansion due to the relatively large areal mass of the Be tamper ( $6 \mu\text{m}$  on each side). In conjunction with the spatially uniform illumination, at these temperatures ( $T_e = 2000 \text{ eV}$ ) and densities ( $n_e \approx 10^{21} \text{ cm}^{-3}$ ) the heat conduction helps maintain a uniform temperature in the Au sample, which is bathed in the hot Be reservoir. The Au foil is optically thin in the direction normal to the surface, and thus radiation transport does not affect the temperature uniformity. Simulations indicate that the density and temperature remain uniform to within  $\sim 10\%$  and  $\sim 5\%$ , respectively. The predicted temperature uniformity is also consistent with spatially resolved temperature measurements obtained from shifting the Thomson probe  $\sim 100 \mu\text{m}$  from the target center, which resulted in no significant difference in  $T_e$ .

Because of the relatively high densities and slow expansion, calculations indicate that the Au sample should remain near steady-state ionization equilibrium during the 2–3 ns following the initiation of the heating pulse. At  $n_e = 6 \times 10^{20}$  and  $T_e = 2 \text{ keV}$ , relaxation times are  $\approx 100 \text{ ps}$  [18], significantly faster than the  $\approx 1 \text{ ns}$  hydrodynamic expansion time. More detailed results from similar 2D simulations illustrating the predicted uniformity and steady-state conditions can be found in Ref. [19].

The Au x-ray emission spectra in the wavelength region  $3.3\text{--}3.9 \text{ \AA}$  were measured with a time-resolved flat Pentaerythritol crystal spectrometer [20]. The resolving power of the instrument is source size limited to  $E/\Delta E \approx 300$ . The  $3.3\text{--}3.9 \text{ \AA}$  wavelength region is dispersed over a 2 cm length onto a time-gated channel plate detector and recorded on Kodak Tmax 3200 film. The spatial and temporal resolutions were  $50 \mu\text{m}$  (on target) and 100 ps, respectively. The spectral data were corrected for the non-linear film response and the variation in sensitivity across the detector.

Shown in Fig. 2 is the measured Au emission spectrum. The spectrum is composed of  $5f\text{--}3d$  supertransition arrays (STAs) that are spectrally well separated by charge state. The two interwoven  $5f_{7/2}\text{--}3d_{5/2}$  and  $5f_{5/2}\text{--}3d_{3/2}$  STAs from charge states germaniumlike (Ge-like)  $\text{Au}^{+47}$  to cobaltlike (Co-like)  $\text{Au}^{+52}$  are clearly identified. These broad STA features are due to transitions between levels with spectator electrons distributed among the  $4l$  ( $0 \leq l \leq 3$ ) orbitals, i.e., Cu-like transitions  $3d^{10}4l\text{--}3d^9j4l5f$  ( $0 \leq l \leq 3$ ) or Zn-like transitions  $3d^{10}4l4l'\text{--}3d^9j4l4l'5f$  ( $0 \leq l, l' \leq 3$ ). The  $j$  value ( $j = 3/2$  or  $5/2$ ) of the  $3d$  hole in the upper level determines the energy splitting of the bands; the  $5f_{5/2}\text{--}3d_{3/2}$  transitions in each ion are  $\sim 85 \text{ eV}$  higher in energy than the corresponding  $5f_{7/2}\text{--}3d_{5/2}$  transitions. Ni-like transitions consist

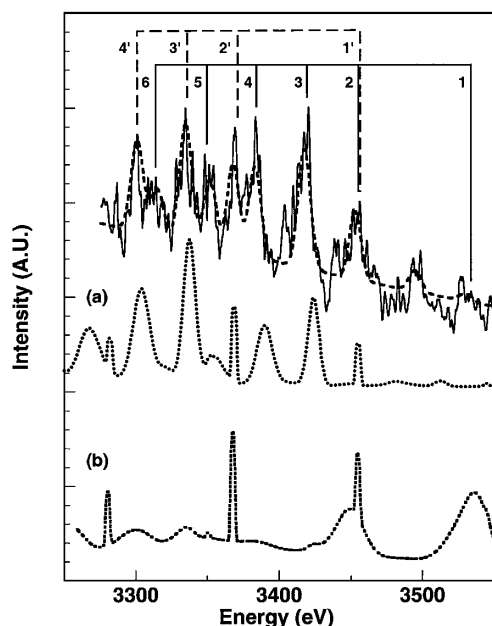


FIG. 2. Au  $5f$ - $3d$  emission spectrum. Co-like to Ge-like features are labeled 1–6. Primed and unprimed numbers refer to  $j = 5/2$ - $3/2$  and  $j = 7/2$ - $5/2$  transition arrays, respectively. The feature at 3490 eV is due to Ni-like  $3d^9 4l$ - $3d^8 4l 5f$  transitions. The dashed line is a multi-Gaussian fit to the data. The dotted lines are calculated spectra from RIGEL (a) with and (b) without two-electron processes included.

mainly of the resonance  $3d^{10}$ - $3d^9 5f$  lines. The weaker  $3d^9 4l$ - $3d^8 4l 5f$  transition arrays are shifted up in energy by  $\sim 50$  eV. The  $5f_{5/2}$ - $3d_{3/2}$  feature for this class of transition at 3490 eV is apparent in Fig. 2, while the associated  $5f_{7/2}$ - $3d_{5/2}$  band blends into the low energy side of the  $5f_{5/2}$ - $3d_{3/2}$  Cu-like transition array.

The population kinetics of the ground state and excited states of each emitting ion were studied using detailed collisional-radiative calculations employing the HULLAC [21] suite of codes. These calculations indicate that, in each ion, the dominant populations are in ground-state or near ground-state levels in which the  $n = 4$  electrons are distributed among excited  $4l$  orbitals. Furthermore, the upper levels involved in the  $5f$ - $3d$  transitions are calculated to be dominantly populated through collisional excitation of the  $3d$  electron in the lower  $3d^{10} 4l$  levels (for various permutations of the  $4l$  electrons). This allows the ionic populations to be determined from the total  $5f$ - $3d$  STA emission strengths, using the calculated ratios of collisional excitation to radiative decay rates between these levels. These ratios are only weakly dependent on the ion charge for these transitions and vary in a similar manner with temperature, providing a relatively model-independent method for determining the charge-state abundances. Corrections due to autoionization and dielectronic recombination between adjacent charge states are also included [21]. These two-electron processes enhance the upper levels of the observed transitions by a small-to-moderate amount, depending on the angular momentum state of the  $4l$  spectator electrons.

The aggregate line strength of each  $5f_{7/2}$ - $3d_{5/2}$  and  $5f_{5/2}$ - $3d_{3/2}$  STA is obtained with a multi-Gaussian fit to the spectrum, assuming a common Gaussian width and using the calculated relative line strengths [22] between  $5f_{7/2}$ - $3d_{5/2}$  and  $5f_{5/2}$ - $3d_{3/2}$  transitions (see Fig. 2). A smooth continuum background is subtracted and the relative strengths of each transition array are determined. The optical depths for the  $5f$ - $3d$  transition arrays are calculated using the measured density and path length through the sample. For simplicity, we assume a spherical, isothermal plasma with the physical distribution of ionization states and allow photoabsorption to redistribute level populations in a self-consistent fashion. At electron density  $6 \times 10^{20} \text{ cm}^{-3}$  and electron and ion temperatures of 2.2 and 2.0 keV, respectively, we find that the Co-, Ni-, Cu-, Zn-, and Ga-like  $5f$ - $3d$  emission features are suppressed by an average of 2%, 12%, 17%, 21%, and 2%, respectively. The STA strengths, adjusted for optical thickness effects, are then used to calculate the populations for each ionic state. Further details on the line transport and collisional-radiative modeling are presented elsewhere [22].

The derived charge-state distribution is shown in Fig. 3. The distribution is peaked near Cu-like Au $^{+50}$  with uncertainties in each charge-state fraction varying from 100% (Co-like) to 30% (Cu-like) as estimated from the variance in fit to the data. Additional uncertainties from the optical depth corrections due to the density uncertainty are much smaller. The average value of this distribution is  $Z^* = 49.3$ . The uncertainty in  $Z^*$  due to uncertainties in each charge-state fraction is  $\pm 0.2$ . Additional uncertainty in  $Z^*$  due to the sensitivity in subtracting the background continuum and from possible inclusion of overlapping emission from other charge states is estimated in a separate study to be  $\pm 0.4$  [22]. Including these contributions to the overall uncertainty yields  $Z^* = 49.3 \pm 0.5$ .

The calculated spectra from the non-LTE code RIGEL [23], using the measured values of  $n_e$  and  $T_e$  as input, are

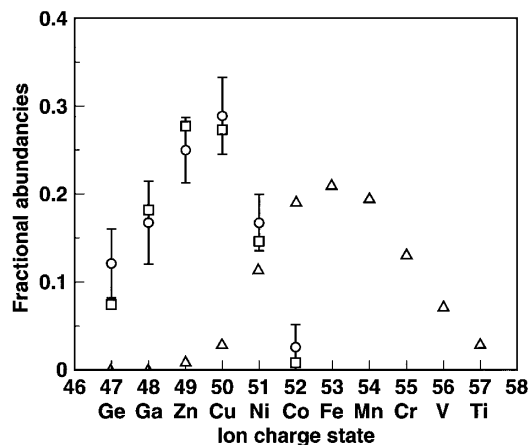


FIG. 3. The derived charge-state distribution for Au (circles). Also shown are results from the code RIGEL, where calculations with (squares) and without (triangles) two-electron processes are shown for comparison.

shown in Fig. 2. RIGEL is a superconfiguration-based [10] collisional-radiative code constructed using hydrogenic supershells, and solved using Monte Carlo techniques. For this calculation, the RIGEL code employed atomic data based on the local density approximation. The predicted value of the average charge is  $Z^* = 49.1$ , and the calculated spectrum shows similar relative intensities to the data, such as between the Ni-, Cu-, and Zn-like features. For comparison, also shown in Fig. 2 is a calculated spectrum in which two-electron processes were not included. In this case, the predicted average charge  $Z^* = 53.3$ . Ni- and Co-like features dominate the spectrum while the lower charge states, Ge-like to Cu-like, are almost negligible.

Comparisons of the calculated and experimental charge-state distributions are shown in Fig. 3. For the case where two-electron processes are included ( $Z^* = 49.1$ ), the peak position and width of the calculated distribution agree well with the data. For the case in which two-electron processes were not included, the distribution is shifted higher by four ionization stages (corresponding to  $Z^* = 53.3$ ), far outside the range of the experimental results.

Effects of the ambient radiation field on the ionization balance and emission spectrum in the Au sample were considered. The 2D LASNEX simulations described above predict that radiation temperature in the relatively thin Au samples remains below 100 eV. Calculations with an applied 100 eV thermal radiation field resulted in no significant difference in the emission spectrum of the  $5f$ - $3d$  transition arrays or in the average charge state ( $<0.1$ ), due to the relatively high threshold for photoionization. Therefore, the ambient radiation field in these thin samples should have little effect on the charge-state distribution or spectral emission features in this wavelength region of interest.

As mentioned above, the optical depth of  $n = 5 - 3$  transitions were taken into account in the analysis, and leads to a small correction in the charge-state distribution. However, the populations of doubly excited states with  $n = 4$  electrons, such as Ni-like  $3d^8 4l 5l'$  levels, may be enhanced through photoabsorption of electrons in  $n = 3$  levels. Radiative decay from these levels would produce enhanced satellite emission for the  $3d^9 4l$ - $3d^8 4l 5f$  transitions, and may explain why the measured intensity of this feature at 3490 eV is higher than predicted from the RIGEL code, which does not include line transport effects.

To summarize, the charge-state distribution in a well-characterized, highly ionized, high- $Z$  plasma has been accurately determined for the first time. We clearly demonstrate that two-electron processes, which significantly lower the average charge state, are required to be consistent with our experimental results.

The authors thank A. Bar-Shalom, A. L. Osterheld, M. J. Eckart, A. Hazi, and R. W. Lee, for helpful discussions, and C. Bruns, E. Hsieh, and J. Ticehurst for technical assistance. This work was performed under the auspices of the U.S. Department of Energy by the Lawrence Liv-

ermore National Laboratory under Contract No. W-7405-Eng-48.

- [1] H. R. Griem, *Phys. Fluids B* **4**, 2346 (1992); see also J. Lindl, *Phys. Plasmas* **2**, 3933 (1995), and references therein.
- [2] C. De Michelis and M. Mattioli, *Rep. Prog. Phys.* **47**, 1233 (1984).
- [3] K. L. Wong, P. T. Springer, J. H. Hammer, C. A. Iglesias, A. L. Osterheld, M. E. Foord, H. C. Bruns, and J. A. Emig, *Phys. Rev. Lett.* **80**, 2334 (1998).
- [4] J. C. Raymond and N. C. Brickhouse, *Astrophys. Space Sci.* **237**, 321 (1996).
- [5] B. K. F. Young, W. H. Goldstein, A. L. Osterheld, R. E. Stewart, G. Charatis, and Gar. E. Busch, *J. Phys. B* **22**, L533 (1989); B. K. F. Young *et al.*, *J. Quant. Spectrosc. Radiat. Transfer* **51**, 417 (1994).
- [6] S. Gary *et al.*, *J. Quant. Spectrosc. Radiat. Transfer* **54**, 155 (1995).
- [7] H. Merdji, T. MiBalla, F. Perrot, J. C. Gauthier, K. Eidmann, and C. Chenais-Popivucis, *Phys. Rev. E* **57**, 1042 (1998).
- [8] S. H. Glenzer *et al.*, *Phys. Rev. Lett.* **82**, 97 (1999).
- [9] W. A. Lokke and W. H. Grasberger, Lawrence Livermore National Laboratory Technical Report No. UCRL-52276, 1977 (unpublished).
- [10] A. Bar-Shalom, J. Oreg, W. H. Goldstein, D. Shvarts, and A. Zigler, *Phys. Rev. A* **40**, 3183 (1989); A. Bar-Shalom and J. Oreg, *Phys. Rev. E* **54**, 1850 (1996).
- [11] B. G. Wilson, J. R. Albritton, and D. A. Liberman, in *Proceedings of the 4th International Workshop on Radiative Properties of Hot Dense Matter, Sarasota, 1990*, edited by W. Goldstein, C. Hooper, J. Gauthier, J. Seely, and R. W. Lee (World Scientific, Singapore, 1991).
- [12] J. Abdallah, Jr., R. E. H. Clark, D. P. Kilcrease, G. Csanak, and C. J. Fontes, in *Atomic Processes in Plasmas*, edited by A. L. Osterheld and W. H. Goldstein, AIP Conf. Proc. No. 381 (AIP, New York, 1996).
- [13] R. W. Lee, J. K. Nash, and Y. Ralchenko, *J. Quant. Spectrosc. Radiat. Transfer* **58**, 737 (1997).
- [14] M. Busquet, *Phys. Fluids B* **5**, 4191 (1993).
- [15] E. M. Campbell, J. T. Hunt, E. S. Bliss, D. R. Speck, and R. P. Drake, *Rev. Sci. Instrum.* **57**, 2101 (1986); *Laser Part. Beams* **9**, 209 (1991).
- [16] S. H. Glenzer *et al.*, *Rev. Sci. Instrum.* **70**, 1789 (1999).
- [17] G. B. Zimmerman and W. L. Kruer, *Comments Plasma Phys. Control. Fusion* **2**, 51 (1975).
- [18] J. R. Albritton and B. G. Wilson, *Phys. Rev. Lett.* **83**, 1594 (1999).
- [19] M. E. Foord *et al.*, *J. Quant. Spectrosc. Radiat. Transfer* **65**, 231 (2000).
- [20] C. A. Back, R. L. Kauffman, P. M. Bell, and J. D. Kilkenny, *Rev. Sci. Instrum.* **66**, 764 (1995).
- [21] A. Bar-Shalom and M. Klapisch, *Comput. Phys. Commun.* **50**, 375 (1988); M. Klapisch, *Comput. Phys. Commun.* **2**, 239 (1971); M. Klapisch, J. Schwob, B. Fraenkel, and J. Oreg, *J. Opt. Soc. Am.* **67**, 148 (1977).
- [22] K. B. Fournier, P. T. Springer, M. E. Foord, and B. G. Wilson (to be published).
- [23] B. G. Wilson (private communication).